RSC Advances

PAPER

Cite this: *RSC Adv.*, 2020, **10**, 9940

Highly-robust, solution-processed flexible transparent electrodes with a junction-free electrospun nanofiber network†

Geon Hwee Kim,‡[a] Hyeonsu Woo,‡[a] Suhyeon Kim,[a] Taechang An*[c] and Geunbae Lim*[ab]

Received 7th December 2019
Accepted 1st March 2020

DOI: 10.1039/c9ra10278g

rsc.li/rsc-advances

Flexible transparent electrodes (FTEs) are widely used in a variety of applications, including flexible displays and wearable devices. Important factors in FTE design include active control of electrical sheet resistance, optical transparency and mechanical flexibility. Because these factors are inversely proportional to one another, it is essential to develop a technique that maintains flexibility while actively controlling the sheet resistance and transparency for a variety of applications. This research presents a new method for fabricating transparent electrodes on flexible polyimide films using electrospinning and copper electroless deposition methods. A flat metal network-based electrode without contact resistance was fabricated by heat treatment and electroless deposition onto the electrospun seed layer. The fabricated FTEs exhibited a transparency exceeding 80% over the entire visible light range and a sheet resistance of less than 10.0 Ω sq^{-1}. Due to the heat treatment process, the adhesion between the metal network and the substrate was superior to other electrospinning-based transparent electrodes. Applicable to the large-area manufacturing process, the standard deviation of the network density of the fabricated large-area FTE was about 1%. This study does not require the polymer casting technique and has further advantages for mass production of electrodes and application to various fields.

Introduction

As modern electronic technologies have developed, transparent films with high electrical conductivity have become necessary. Transparent conductive electrodes are used in displays,[1,2] light-emitting diodes (LEDs),[3] touch screens,[4,5] solar cells[6] and other devices. In addition to high optical transparency and electrical conductivity, transparent electrodes also have important advantages in terms of manufacturing costs, chemical and thermal stability, and mechanical strength.[7] In recent years, as flexible display technology has developed, the flexibility of electrodes has come to represent an important performance indicator. Conventional transparent electrodes are mostly made using a transparent conductive oxide, where indium tin oxide (ITO) is typically used. ITO-based transparent electrodes are limited by their high cost, low optical permeability in the ultraviolet region, and brittleness.[8]

To overcome the disadvantages of ITO transparent electrodes, techniques for fabricating transparent electrodes using graphene,[9] carbon nanotubes (CNTs),[10,11] metal nanowire networks[12,13] and conducting polymers[14] have been studied. Electrical conductivity was characterized by depositing the conductive materials onto a transparent film using chemical vapor deposition,[15] sputtering[16] or spin coating.[17] As a result, the films were more flexible than ITO, but there were some issues; the conductivity of the deposition method was lowered by the contact resistance of the network junctions[18] and the conductive material did not strongly adhere to the transparent film. Therefore, it is necessary to fabricate an FTE with excellent mechanical strength and high electrical conductivity. Recently, there have been attempts to overcome the aforementioned disadvantages by inserting a conductive material into the polymer.[19–21] The method of inserting the electrode inside a transparent film by coating the dissolved polymer onto conductive material greatly increases the mechanical strength of the transparent electrode. However, coating the dissolved polymer is difficult to achieve in mass production, and reduced conductivity remains due to the junction of the network. To remove the junction, mechanical pressing,[22,23] annealing[24] and

[a]*Department of Mechanical Engineering, Pohang University of Science and Technology (POSTECH), 77, Cheongam-ro, Nam-gu, Pohang-si, Gyeongsangbuk-do, 37673, Republic of Korea. E-mail: limmems@postech.ac.kr; Fax: +82-54-279-0479; Tel: +82-54-279-2186*

[b]*Department of Integrative Bioscience and Biotechnology, Pohang University of Science and Technology (POSTECH), 77, Cheongam-ro, Nam-gu, Pohang-si, Gyeongsangbuk-do, 37673, Republic of Korea*

[c]*Department of Mechanical Design Engineering, Andong National University, 1375, Gyeongdong-ro, Andong-si, Gyeongsangbuk-do, 36729, Republic of Korea. E-mail: tcmerias@andong.ac.kr; Tel: +82-54-820-7767*

† Electronic supplementary information (ESI) available. See DOI: 10.1039/c9ra10278g

‡ These authors equally contributed to this work.

optical sintering[25] have been studied. These methods cause mechanical stresses in the substrate, and the metal network may be partially melted to form a bead. Therefore, there is a need to develop a new production technology for transparent electrodes with excellent mechanical strength, high electrical conductivity and flexibility.

Transparent electrode manufacturing technologies using electrospinning are actively being developed. Electrospinning is a popular and economical technique for manufacturing ultra-thin nanofibers with features such as long nanofiber length, high surface-area to volume ratio and high porosity. These advantages are exploited in the manufacture of gas sensors,[26] filters,[27] and batteries[28] and, recently, in the fabrication of transparent electrodes. An *et al.*[29] collected polymer fibers by electrospinning and metallized them using copper electrodeposition, to transfer the electrodes to the desired substrate. Hsu *et al.*[30] demonstrated the electrospinning of $SnCl_2$-embedded nanofibers directly onto a hydrophobic substrate, which was then metallized by electroless deposition. However, these techniques require transfer of the electrodes fabricated in a floating state to a substrate, or that they have a polymer core. The currently used transfer process has adhesion problems at the interface between the substrate and the electrodes, and the complexity of the process imposes restrictions on substrate shape and large-area manufacturing. If the polymer core layer remains after the process, the conductivity of the fabricated electrode network will be reduced.

In this study, we developed a new method for fabricating two-dimensional (2D) transparent electrodes on flexible polymer films using electrospinning and copper electroless deposition.[31] A random network was formed by electrospinning a polymer solution containing palladium ions onto a transparent polyimide (PI) film. The electrospun palladium-embedded polymer network was heat-treated to form a seed layer for the electrode, and a subsequent copper nanofiber network was fabricated by copper electroless deposition. The metal network of the transparent electrode has a 2D junction without contact resistance. The fabrication method of the electrospinning and electroless deposition-based FTE proposed in this study is a direct patterning-based technology that does not require lift-off or transfer process. Using a lift-off or transfer process basically means moving the nanostructure to another substrate, which is one of the causes of defects and uneven performance. The direct patterning-based method of this study has an important advantage that it can basically reduce the number of process steps compared to lift-off or transfer process. As a result, it was verified that the FTE having a relatively uniform performance could be produced reproducibly. Also, the entire process is done without a vacuum process or electrodeposition, this method can be used for large-scale production.

The fabricated electrodes were confirmed to have a transparency of over 90% in the entire visible light region, the metal network junction was perfectly formed, and the electrical sheet resistance was small. Using repetitive bending and tape peeling tests, the mechanical strength of the electrode was scrutinized.

Experimental section

Materials

The PI films were purchased from Kolon Industry. Polyvinylpyrrolidone (PVP, AR, molecular weight, 1 300 000) powder was purchased from Sigma-Aldrich. Formaldehyde solution (35.0%) and *N*,*N*-dimethylmethanamide (DMF, AR, 99.5%) were purchased from Samchun. Ammonium tetrachloropalladate ($(NH_4)_2PdCl_4$) was purchased from Dongjin PGMs Chemical Company. Sodium hydroxide (NaOH) and potassium sodium (+)-tartrate tetrahydrate ($KNaC_4H_4O_6 \cdot 4H_2O$) were purchased from Kanto Chemical Co., Inc. Copper(II) sulfate pentahydrate ($CuSO_4 \cdot 5H_2O$) was purchased from Daejung Chemicals & Metals Co., Ltd. All reagents were used as received without further purification.

Seed layer fabrication

A flexible PI film and polymer solution with palladium ions were prepared for electrospinning (Fig. 1A). The polymer solution was prepared by adding 0.15 g mL^{-1} PVP and 0.03 g mL^{-1} $(NH_4)_2PdCl_4$ to DMF, with stirring at 600 rpm using a magnetic stirrer for 2 h. Electrospinning was performed at room temperature with low humidity (Fig. 1B). The gap between the tip and collector was fixed at 10 cm, and the applied voltage was 9 kV. The flow rate of the polymer solution was 5 μL min^{-1}. A motorized biaxial stage was set up to control the amount of nanofiber on the flexible substrate. Once the nanofiber was collected on the flexible substrate, the polymer was decomposed and calcinated in air at 310 °C to form a seed layer for electroless deposition (Fig. 1C).

Copper electroless deposition

The electroless deposition used in this experiment is copper reduction deposition. Copper electroless deposition solution was prepared by adding 0.1 mL mL^{-1} formaldehyde (HCHO), 40 mg mL^{-1} NaOH, 140 mg mL^{-1} $KNaC_4H_4O_6 \cdot 4H_2O$, and 30 mg mL^{-1} $CuSO_4 \cdot 5H_2O$ to deionized water (Fig. 1D). The chemical equation of copper electroless deposition is as follows:

$$Cu^{2+} + 2HCHO + 4OH^- \rightarrow Cu + 2HCOO^- + 2H_2O + 2H_{ads} \quad (1)$$

The $CuSO_4 \cdot 5H_2O$ was used to add copper ions, formaldehyde as a reducing agent, and NaOH as a pH-adjusting agent. When the pH is elevated above 11 by the NaOH, the formaldehyde generates electrons through a strong reduction reaction. The generated electrons are then combined with the Cu ions to precipitate onto the palladium catalyst for plating. The electroless deposition solution should be used immediately after preparation, as the formaldehyde is consumed by the Cannizzaro reaction (eqn (2)) and the pH is reduced, resulting in a slower precipitation reaction.

$$NaOH + 2HCHO \rightarrow HCOONa + CH_3OH \quad (2)$$

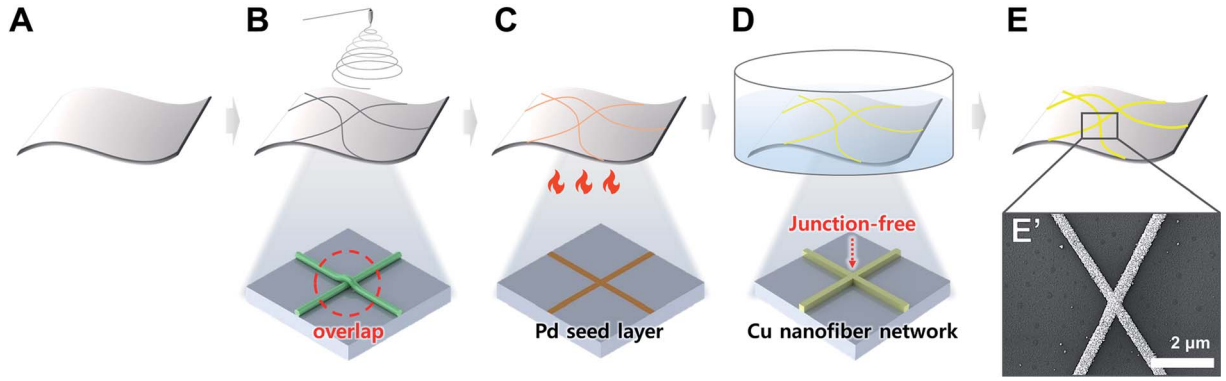

Fig. 1 Schematics of the flexible transparent electrode (FTE) fabrication process. (A) Preparation of bare flexible polyimide film. (B) Electrospinning of nanofibers containing palladium ions. (C) Calcination to degrade the polymer component of the nanofibers. (D) Copper electroless deposition by palladium catalyst. (E) Copper nanofibers network-based FTE. (E′) Scanning electron microscopy (SEM) image of FTE surface.

The amount of copper electrode formed was adjusted by controlling the reaction time of the flexible substrate at the seed layer (Fig. 1E).

Characterization

The morphology of the copper nanofibers was analyzed using scanning electron microscopy (SEM) with energy dispersive X-ray spectroscopy (EDS; LYRA 3 XMH; TESCAN). The width and density of the nanofibers was determined using ImageJ (NIH). The density distribution of the nanofiber network was determined using MATLAB (Mathworks). The morphology and thickness of the nanofibers were analyzed using atomic force microscopy (AFM) in tapping mode (Multimode NanoScope III; Digital Instruments). The transmittance of the electrodes was analyzed by ultraviolet-visible (UV-Vis) spectrophotometry (model 8453; Agilent); the reference transmittance was set to that of the glass substrate. The sheet resistance of the electrodes was analyzed by the four-point probe technique using a SourceMeter (models 2182 A and 6221; Keithley). The line resistance of the electrodes was measured using a digital multimeter (15B+; FLUKE).

Results & discussion

Fig. 2 shows the morphology of the copper nanofibers synthesized by copper electroless deposition of electrospun nanofibers. Fig. 2A is an SEM image of a palladium-embedded PVP nanofiber electrospun onto a PI film; overlapping of nanofibers is observed, which causes the contact resistance to lower the electrical performance. Fig. 2B is an SEM image of the electrospun nanofibers after a heat treatment. The contact point of the nanofibers is partially melted by the heat treatment, to remove the overlap. In this step, the PVP component of the nanofiber has degraded and adhered to the substrate to form a seed layer. Fig. 2C is an SEM image of a copper nanofiber formed by electroless deposition onto a heat-treated palladium-embedded seed layer. Unlike previous studies of transparent electrodes using electroless deposition, the conductive nanofibers have no overlap or height difference at the junctions. The palladium ions contained within the seed layers are used as a catalyst, to which the copper ions are precipitated to form copper nanofibers. Since the copper network is formed on the seed layers where the overlap is removed through heat treatment, there is no overlap at the junction.

Other studies have removed the contacts by mechanical and thermal methods to lower the contact resistance of the metal network. Tokuno *et al.*[12] fabricated a transparent electrode by mechanically pressing Ag nanowires to form a network connection. Langley *et al.*[32] formed a contact connection by melting the metallic nanowire junctions using a thermal annealing process. However, it has been reported that metal beads can be formed by the metallic nanowires when a large amount of thermal energy is transferred. Lee *et al.*[33] locally heated the junctions in a laser nano-welding process to form a network connection. In this study, after removing the nanofiber overlap of the seed layer, a metal network is grown to form a non-overlapping connection. Since there is no mechanical/thermal stress applied directly to the metal network; this does not affect the properties of the metal component.

The EDS analysis was performed to confirm that copper nanofibers were formed through electroless deposition. In Fig. 2D and D′, the copper was detected along the nanofiber. Fig. 2E is an AFM image of fabricated copper nanofibers; the peak height of the copper nanofibers is 113 nm and there is no difference in height at the junction point. The SEM and AFM images show that the height of the nanofibers is constant at the junction, without defects. The 2D copper nanofiber network in this research is different from the cylindrical nanofibers of previous research.[34] Based on the SEM images, the morphology of the copper nanofibers was analyzed in relation to electroless deposition time. Fig. 2F is a graph plotting the electroless deposition time against the thickness of the nanofibers. The investigation of electroless deposition time was performed from 1 to 6 minutes, and the thickness was found to be 70 and 240 μm at 1 and 6 minutes, respectively. The thickness of the nanofibers is proportional to the synthesis time, with an average growth rate of 33.5 nm min^{-1}. The collecting time of the

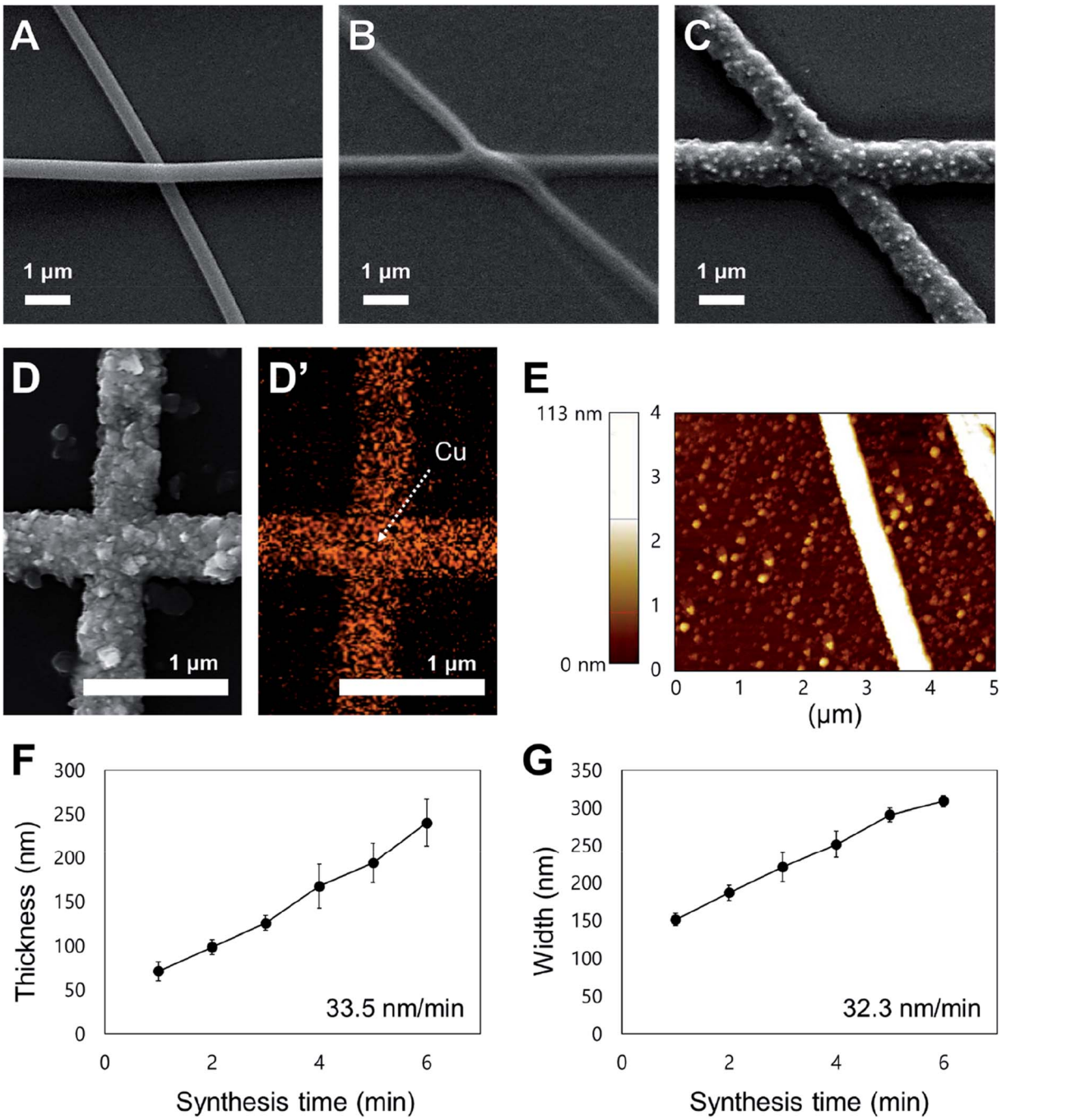

Fig. 2 Analysis of the copper nanofiber fabrication conditions and morphology. (A) SEM image of electrospun palladium-embedded polyvinylpyrrolidone (PVP) nanofibers. (B) SEM image of electrospun PVP nanofibers degraded by heat treatment. (C) SEM image of electroless deposited copper nanofibers. (D) Component analysis map used to analyze the fabricated copper nanofibers *via* energy dispersive X-ray spectroscopy (EDS). The red spots on the component analysis map shows the copper component. (E) Atomic force microscopy (AFM) image showing copper nanofiber thickness and morphology. (F) Graph of electroless deposition time against the thickness of the nanofibers ($n = 5$, mean ± standard error). (G) Graph of electroless deposition time against the width of the nanofibers ($n = 5$, mean ± standard error).

nanofibers during the electrospinning process is correlated with the density of the nanofibers and is not related to the thickness change. Fig. 2G graphs the electroless deposition time against the width of nanofibers. The investigation of electroless deposition time was performed from 1 to 6 minutes, and the width was observed to be 150 and 310 μm at 1 and 6 minutes, respectively. The width of the nanofibers is proportional to the synthesis time, with an average growth rate of 32.3 nm min^{-1}. These results show that both the thickness and width of the nanofibers can be controlled through the electroless deposition process, and that the nanofiber network is a 2D structure with no contact resistance. The density and

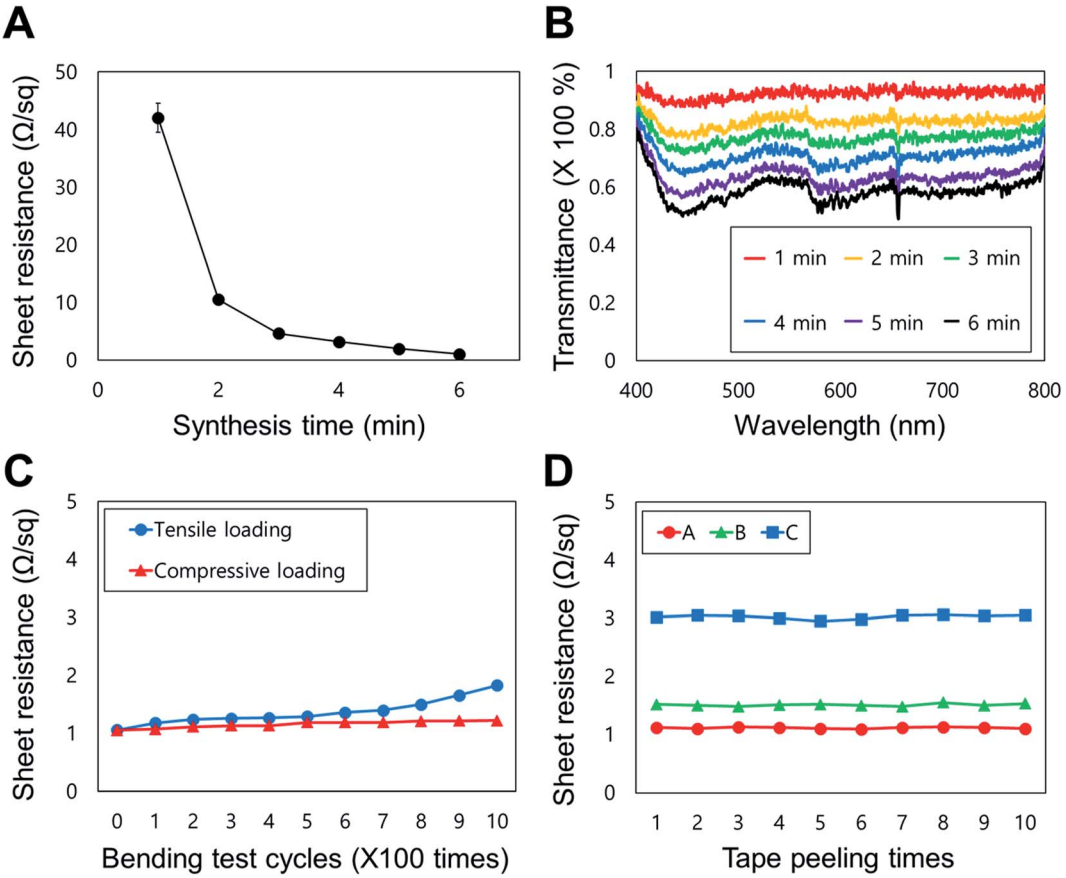

Fig. 3 Analysis of the electrical, optical and mechanical properties of FTEs. (A) Graph of electroless deposition time against the sheet resistance of FTEs ($n = 5$, mean ± standard error). (B) Graph of transmittance against the sheet resistance (in the visible range: 400–800 nm). (C) Graph of the number of bending cycles against the sheet resistance. (D) Commercial 3M Scotch Tape was directly attached to the electrode and repeatedly detached and reapplied to measure the change in sheet resistance ($n = 3$).

morphology of nanofiber networks can be actively controlled for better application while minimizing both the electrical sheet resistance and optical transmittance reduction.

Fig. 3 shows the electrical, optical, and mechanical properties of the FTE based on a copper nanofiber network. Fig. 3A graphs the sheet resistance change of the FTE by the electroless deposition time; the sheet resistance decreases as the synthesis time increases. As the electroless deposition time increases, the cross-sectional area of the conductor increases due to the increase in width and thickness of the copper nanofiber, causing the sheet resistance to decrease. The sheet resistance decreased fastest between 1 and 2 minutes of synthesis, and was less than 10 Ω sq^{-1} after 2 minutes. The sheet resistance was approximately 1 Ω sq^{-1} when the synthesis time exceeded 6 minutes. Fig. 3B graphs the transmittance (wavelength range: 400–800 nm) of the FTE by the sheet resistance. Fig. 3A and B show that the longer the synthesis time, the lower the sheet resistance and transmittance. The FTEs have a transmittance of approximately 90% at 1 minute (sheet resistance of approximately 40 Ω sq^{-1}) and a transmittance of approximately 60% at 6 minutes (sheet resistance of approximately 1 Ω sq^{-1}). By varying the electroless deposition time of a sample with the same nanofiber density, the sheet resistance value corresponding to each transmittance can be adjusted. In addition, by changing the electrospinning performance time, the transparency can be adjusted according to various nanofiber densities.

Fig. 3C shows the change in sheet resistance by the number of bends of the FTE. The change in sheet resistance was measured by bending the FTE 1000 times (bending radius = 5 mm) with the copper nanofiber network located on the inside (compressive loading) and outside (tensile loading) face. When the conductive surface was on the inside surface of the bend, the sheet resistance increased by 0.2 Ω sq^{-1} and the final value was 1.2 Ω sq^{-1}. When the conductive surface was on the outside surface of the bend, the sheet resistance increased by 0.8 Ω sq^{-1}, with a final value of 1.8 Ω sq^{-1}. These results indicate that the sheet resistance values do not change significantly by bending direction. With outward bending, the sheet resistance is increased by 80% of the initial value, but the absolute value is 1.8 Ω sq^{-1}, which is acceptable for electrode applications. The results show that the FTEs have bending durability in both directions and are applicable to flexible electronics. In previous studies, electrodes fabricated using electrospinning exhibited limited mechanical strength, because the cylindrical nanofibers were formed on the target substrate. However, in this study, excellent adhesion between the substrate and the nanofiber was

observed because the electrode network was formed by electroless deposition onto a heat-treated nanofiber seed layer. To demonstrate this, commercially available 3M Scotch Tape was attached to the electrode surface and repeatedly detached (Standard test methods for measuring adhesion by tape test, ASTM D3359-02) to measure changes in the sheet resistance (Fig. 3D); after 10 repetitions, the sheet resistance of the electrode was largely unchanged (approximately 2% change). This result shows that the FTE can maintain its performance in a multilayer bonding structure, so could be applied to a wearable device.

In order to verify the stability of the fabricated FTE, autoclave, sonication, and long-term stability experiments were additionally performed and analyzed. First, the FTE performance was evaluated through autoclave (121 °C, 20 min) treatment in order to verify the stability of the FTE in a high temperature/high pressure/humid environment. The transparency (visible light, 400–800 nm) and sheet resistance before and after the autoclave treatment were compared (Fig. S1A†). The transparency and sheet resistance values before autoclave treatment were 81.3% and 4.57 Ω sq^{-1}, respectively, and after treatment, they were 80.0% and 4.66 Ω sq^{-1}, respectively. Comparing the two results, the change in transparency and sheet resistance due to the autoclave treatment is very small. Although there is a slight difference, both transparency and sheet resistance change are within the standard deviation. This experiment confirmed the stability of the FTE at high temperature/high pressure/high humidity environment. Next, the characteristics were evaluated by sonication treatment (350 Watt, 40 kHz) to verify the stability under ultrasonic vibration of the FTE (Fig. S1B†). The transparency and sheet resistance values before the sonication treatment were 82.13% and 4.03 Ω sq^{-1}, respectively, and after the treatment, they were 80.40% and 4.04 Ω sq^{-1}, respectively. Comparing the two results, it shows that the transparency and the sheet resistance change according to the sonication treatment are very small. This experiment confirmed the stability under ultrasonic vibration of the FTE. Finally, an experiment for verifying the long-term stability of the FTE was analyzed. The resistance value was measured immediately after fabrication of the FTE (7 cm × 1 cm) and after 4 months of storage (room temperature, open space, temperature: 8.6–21 °C, humidity: 49–65%) (Fig. S2A–C†). The resistance value immediately after fabrication was 14.8 Ω, and the value after 4 months was 17.7 Ω, resulting in an increase of about 14%. Although the value increased slightly, the fact that copper nanofiber networks exposed to open spaces at room temperature maintained transparency and conductivity without damage for more than four months shows excellent long-term stability results. These three additional tests validate the stability of the FTE, which will ensure the durability of the electrode in various applications.

In order to verify the reproducibility of the FTE fabrication method, five samples were produced under the same conditions and analyzed (Fig. S3†). The electroless deposition time of the samples were set to 3 minutes (see Fig. 3A and B). Transparency measurements of the five samples showed an overall average of 83.25% (max: 85.18%, min: 81.09%) and a standard deviation of 1.60. The sheet resistance values showed an overall average of 4.29 Ω sq^{-1} (max: 4.78 Ω sq^{-1}, min 4.03 Ω sq^{-1}) and a standard deviation of 1.23. This result is almost the same as the data for 3 min of electroless deposition in Fig. 3A and B, and it is shown that all five samples have very similar characteristics. This experiment shows the reproducibility of the electrospinning and electroless deposition based FTE fabrication method proposed in this study.

Fig. 4 shows an application of the FTE based on the optical and electrical properties. Fig. 4A is an optical image of the change in transparency during the FTE fabrication process. The FTE fabrication is shown in Fig. 4A (1)–(4). Sample (1) is the bare PI film and sample (2) is the electrospun palladium-embedded PVP nanofibers formed on the PI substrate. In sample (3), the electrospun PVP nanofibers are degraded by the heat treatment to form a seed layer. In sample (4), the copper nanofiber network produced by electroless deposition is formed onto the seed layer to complete an FTE. Comparing the images of samples (1) to (4), the transparency does not change during the fabrication process. A copper nanofiber network with a width of 1 μm is formed on the PI film surface and does not affect the optical properties of the PI film. Since the heat treatment temperature is lower than the glass transition temperature of the PI film, the mechanical and optical properties of the PI film are not affected. This result indicates that the characteristics of the substrate are maintained during the manufacturing process from (1) to (4), and the transparency does not change.

Fig. 4B is an optical image of a large-area FTE in which a copper nanofiber network is formed on a 6 inch rounded rectangular PI substrate. The copper nanofiber network was formed on the PI film with electrospinning, using a motorized stage over a large area. Fig. 4B′ is an SEM image of a large-area FTE fabricated. This direct electrospinning method can easily achieve fabrication of large area electrodes when compared to conventional transfer processes that require complex fabrication conditions. When fabricating large-area FTEs, it is important to maintain an uniform density of the copper nanofiber networks across the entire electrode area. In Fig. 4C, the uniformity of the large-area FTE nanofiber network density was measured and analyzed. Sample (a) corresponds to the red graph (1 m electroless deposition) of Fig. 3B, and sample (b) corresponds to the green graph (3 m electroless deposition). For each large-area FTE, 20 images were taken at intervals of 0.5 cm over an area of 10 cm × 10 cm, vertically and horizontally, resulting in a total of 400 images (20 × 20). The density of the nanofiber network was analyzed using an ImageJ algorithm and the three-dimensional graph was displayed using MATLAB. For each sample, it was confirmed that the nanofiber network density was relatively uniform over the entire area, and for the different types of samples, the density distribution greatly varied from sample to sample according to the fabrication condition. Fig. 4D is a graph showing the measured density values of samples (a) and (b) of Fig. 4C. Sample (a) has an average density of 4.9% (maximum: 6.3%, minimum: 3.3%, standard deviation: 0.6%), and sample (b) has an average density of 18.2% (maximum: 21.0%, minimum: 15.8%, standard deviation: 1.1%). Since each sample has a standard deviation of approximately 1%, it can be said that the nanofiber

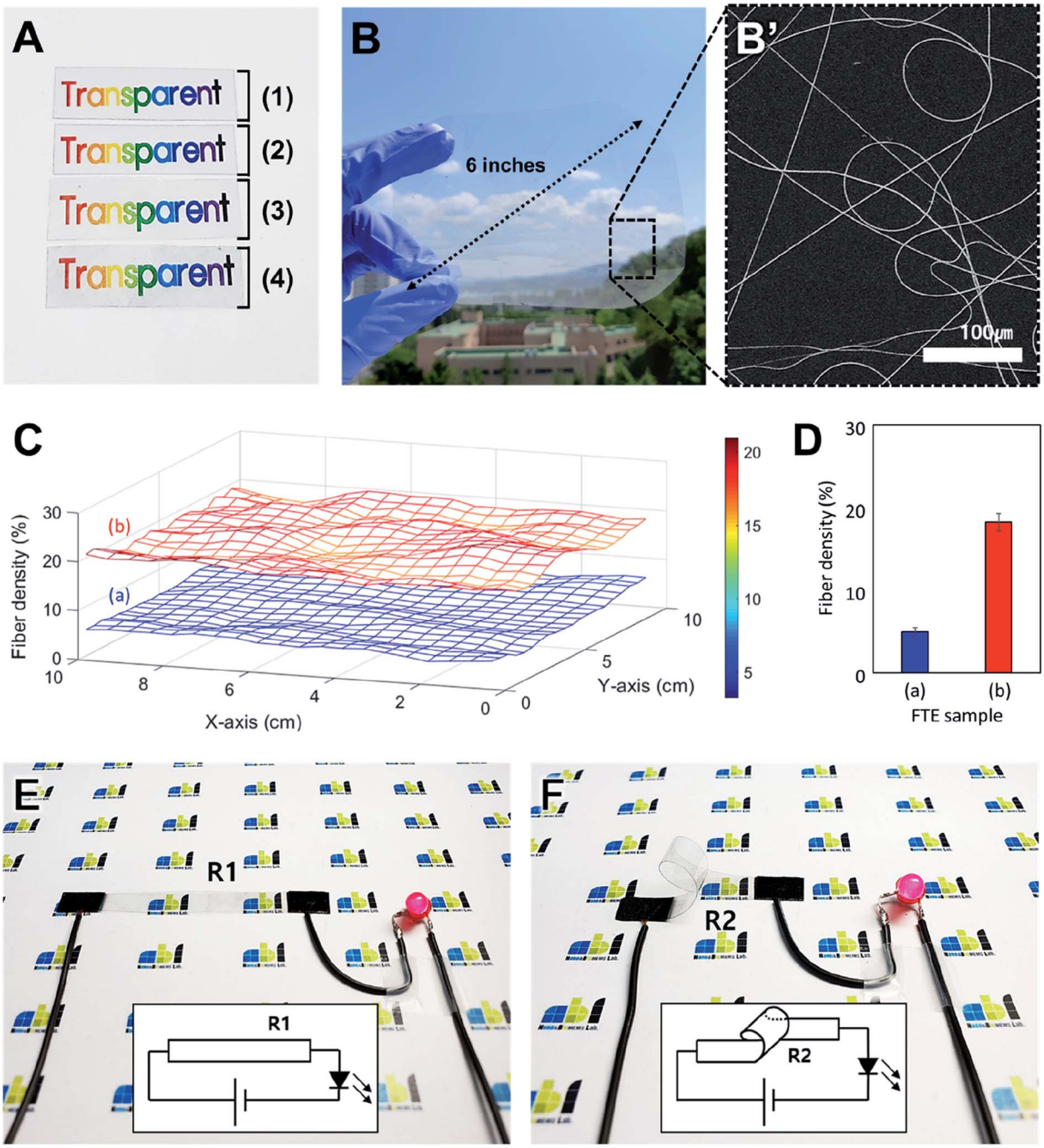

Fig. 4 The optical and electrical properties of FTEs. (A) Optical image of transparency change during the FTE fabrication process. (B) The FTEs formed evenly over the 6 inch rounded rectangular substrate (width: 12 cm; height: 10 cm). (B′) SEM image of large-area FTE. (C) 3-D graph of copper nanofiber density distribution of large-area FTE. (D) Numerical analysis graph about (C). (E) Use of the FTE as a flat LED interconnector. (F) Use of the FTE as a bendable light-emitting diode (LED) interconnector.

network density of the large-area FTE is relatively uniform over the entire region. This means that the seed layer fabricated by electrospinning is formed uniformly, and that the copper nanofibers grow evenly in the solution process such as electroless deposition. The electrode fabrication method proposed in this study shows its applicability to large area processes and shows a uniform distribution over the entire area of the fabricated FTE.

Fig. 4E and F shows an LED driven by a configured circuit of FTEs. In Fig. 4E, a flat, rectangular FTE (width: 10 cm; height: 2 cm) with a copper network on the top surface was used for circuit configuration. When a wire was connected to both ends of the flat electrode and 3 V was applied, a red LED was turned on. When the resistance (R1) was measured using a multimeter at both ends of a flat electrode, it recorded a value of 15 Ω. In the next step, a 360 degree bent electrode with the copper network on the

inside surface was connected to the circuit. Wires were connected to both ends of the bent FTE, and when 3 V was applied, the red LED turned on as in the previous experiment (Fig. 4F). When the resistance (R2) at both ends of the bent FTE was measured, it recorded a value of 16 Ω. The results show that the electrode performance is maintained despite bending the electrode, and the low resistances are suitable for flexible circuit configuration.

Conclusion

In conclusion, we developed an FTE fabrication technology based on electrospinning that can overcome the limitations of conventional transparent electrode fabrication and provide mechanical flexibility. A random nanofiber network is formed on a flexible substrate using electrospinning and heat-treated to form a thin seed layer. The optimization of electrospinning is difficult for polyimide films with relatively hydrophobic environments, but the results of this study show that the optimization of conditions for forming nanofiber networks stably on the polymer film is achieved. Copper nanofibers were fabricated by electroless deposition onto the seed layer, to form electrodes. These processes do not affect the mechanical or optical properties of the PI film; the transparency of the PI film is maintained. The sheet resistance and transmittance of the electrodes were tuned by controlling the electroless deposition time. This technology has improved the mechanical and electrical performance of FTEs compared to conventional technologies, because the polymer component is removed by the heat treatment and there is no contact resistance at the nanofiber junctions. Since the seed layer is formed by electrospinning, electrodes can be formed on complicated surfaces and substrates of various materials. The electrode performance is maintained in both bending directions, and the adhesive force at the interface between the substrate and the copper nanofibers is strong. These attributes are suited to wearable devices having a multilayer structure. A direct electrospinning process was used to confirm that large-area processing is possible, and the density of nanofibers is constant for large-area electrodes. Most importantly, FTEs were fabricated by forming the conductive network on a polymer substrate called polyimide. Forming the conductive network on the polymer opens up a lot of possibilities in the applications. Representatively, the conductive network is formed on the stretchable substrate in the future, thereby opening up the possibility of manufacturing the stretchable transparent electrode. The FTE fabrication technology proposed in this study can be applied to various fields, as it is capable of large-area and mass production and shows mechanical, electrical and optical characteristics suitable for practical industrial application. In particular, it will be extended to core technologies for developing next-generation wearable devices such as stretchable electronics.

Conflicts of interest

There are no conflicts to declare.

Acknowledgements

This research was supported by the convergence technology development program for bionic arm through the National Research Foundation of Korea (NRF) funded by the Ministry of Science & ICT (No. 2017M3C1B2085309). This work was supported by the National Research Foundation of Korea (NRF) grant funded by the Korea government (No. 2019R1H1A2077489 & No. 2020R1A2C2007017).

References

1 D. S. Hecht, L. Hu and G. Irvin, *Adv. Mater.*, 2011, **23**, 1482–1513.
2 D. Yin, Z. Y. Chen, N. R. Jiang, Y. F. Liu, Y. G. Bi, X. L. Zhang, W. Han, J. Feng and H. B. Sun, *Org. Electron.*, 2020, **76**, 105494.
3 L. Li, Z. Yu, W. Hu, C. H. Chang, Q. Chen and Q. Pei, *Adv. Mater.*, 2011, **23**, 5563–5567.
4 S. Bae, H. K. Kim, Y. Lee, X. Xu, J.-S. Park, Y. Zheng, J. Balakrishnan, D. Im, T. Lei, Y. Il Song, Y. J. Kim, K. S. Kim, B. Özyilmaz, J.-H. Ahn, B. H. Hong and S. Iijima, *Nat. Nanotechnol.*, 2009, **5**, 574–578.
5 G. Tang and B. Tang, *SN Appl. Sci.*, 2020, **2**, 1–9.
6 Z. Yu, L. Li, Q. Zhang, W. Hu and Q. Pei, *Adv. Mater.*, 2011, **23**, 4453–4457.
7 D. Langley, G. Giusti, C. Mayousse, C. Celle, D. Bellet and J. P. Simonato, *Nanotechnology*, 2013, **24**, 452001.
8 D. Angmo and F. C. Krebs, *J. Appl. Polym. Sci.*, 2013, **129**, 1–14.
9 K. S. Kim, Y. Zhao, H. Jang, S. Y. Lee, J. M. Kim, K. S. Kim, J.-H. Ahn, P. Kim, J.-Y. Choi and B. H. Hong, *Nature*, 2009, **457**, 706–710.
10 A. Du Pasquier, H. E. Unalan, A. Kanwal, S. Miller and M. Chhowalla, *Appl. Phys. Lett.*, 2005, **87**, 1–3.
11 J. Chen, W. Xiao, T. Hu, P. Chen, T. Lan, P. Li, Y. Li, B. Mi and Y. Ma, *ACS Appl. Mater. Interfaces*, 2020, **12**, 5885–5891.
12 T. Tokuno, M. Nogi, M. Karakawa, J. Jiu, T. T. Nge, Y. Aso and K. Suganuma, *Nano Res.*, 2011, **4**, 1215–1222.
13 R. Zhang, Y. Liao, Y. Zhou and J. Qian, *J. Nanopart. Res.*, 2020, **22**, 39.
14 Y. Xia, K. Sun and J. Ouyang, *Adv. Mater.*, 2012, **24**, 2436–2440.
15 J. Sun, M. T. Cole, N. Lindvall, K. B. K. Teo and A. Yurgens, *Appl. Phys. Lett.*, 2012, **100**, 022102.
16 D. Ebner, M. Bauch and T. Dimopoulos, *Opt. Express*, 2017, **25**, A240.
17 S. Yadav and I. Kaur, *RSC Adv.*, 2016, **6**, 78702–78713.
18 R. Song, X. Li, F. Gu, L. Fei, Q. Ma and Y. Chai, *RSC Adv.*, 2016, **6**, 91641–91648.
19 H. J. Yun, S. J. Kim, J. H. Hwang, Y. S. Shim, S. G. Jung, Y. W. Park and B. K. Ju, *Sci. Rep.*, 2016, **6**, 34150.
20 D. S. Ghosh, T. L. Chen, V. Mkhitaryan and V. Pruneri, *ACS Appl. Mater. Interfaces*, 2014, **6**, 20943–20948.
21 S. B. Singh, T. Kshetri, T. I. Singh, N. H. Kim and J. H. Lee, *Chem. Eng. J.*, 2019, **359**, 197–207.

22 W. Gaynor, G. F. Burkhard, M. D. McGehee and P. Peumans, *Adv. Mater.*, 2011, **23**, 2905–2910.
23 T. Xu, C. Gong, S. Wang, H. Lian, W. Lan, G. Lévêque, B. Grandidier, J. Plain, R. Bachelot, B. Wei and F. Zhu, *Sol. RRL*, 2020, **1900522**, 1900522.
24 R. E. Triambulo, H. G. Cheong and J. W. Park, *Org. Electron.*, 2014, **15**, 2685–2695.
25 E. C. Garnett, W. Cai, J. J. Cha, F. Mahmood, S. T. Connor, M. Greyson Christoforo, Y. Cui, M. D. McGehee and M. L. Brongersma, *Nat. Mater.*, 2012, **11**, 241–249.
26 S. K. Lim, S. H. Hwang, D. Chang and S. Kim, *Sens. Actuators, B*, 2010, **149**, 28–33.
27 S. K. Hong, S. Bae, H. Jeon, M. Kim, S. J. Cho and G. Lim, *Nanoscale*, 2018, **10**, 3037–3045.
28 A. Di Blasi, C. Busaccaa, O. Di Blasia, N. Briguglio, G. Squadrito and V. Antonuccia, *Appl. Energy*, 2017, **190**, 165–171.
29 S. An, H. S. Jo, D.-Y. Kim, H. J. Lee, B.-K. Ju, S. S. Al-Deyab, J.-H. Ahn, Y. Qin, M. T. Swihart, A. L. Yarin and S. S. Yoon, *Adv. Mater.*, 2016, **28**, 7149–7154.
30 P.-C. Hsu, D. Kong, S. Wang, H. Wang, A. J. Welch, H. Wu and Y. Cui, *J. Am. Chem. Soc.*, 2014, **136**, 10593–10596.
31 G. H. Kim, J. H. Shin, T. An and G. Lim, *Sci. Rep.*, 2018, **8**, 13581.
32 D. P. Langley, M. Lagrange, G. Giusti, C. Jiménez, Y. Bréchet, N. D. Nguyen and D. Bellet, *Nanoscale*, 2014, **6**, 13535–13543.
33 J. Lee, P. Lee, H. Lee, D. Lee, S. S. Lee and S. H. Ko, *Nanoscale*, 2012, **4**, 6408–6414.
34 Y. K. Fuh and L. C. Lien, *Nanotechnology*, 2013, **24**, 55301–55308.